ACS OMEGA

http://pubs.acs.org/journal/acsodf

Article

$Zn_{0.8}Cd_{0.2}S$ Hollow Spheres with a Highly Dispersed Ni Dopant for Boosting Photocatalytic Hydrogen Generation

Ying Luo, Xiaohui Zhang, Cheng Huang, Xiaole Han, Qingqing Jiang, Tengfei Zhou, Haijian Yang, and Juncheng Hu*

Cite This: *ACS Omega* 2021, 6, 13544−13553

Read Online

ACCESS | Metrics & More | Article Recommendations | Supporting Information

ABSTRACT: Facilitating charge separation and increasing surface active sites have always been the goals of photocatalysis. Herein, we synthesized a Ni-doped $Zn_{0.8}Cd_{0.2}S$ hollow sphere photocatalyst with a facile one-step hydrothermal method. Energy-dispersive spectroscopy mapping showed the high dispersion of Ni ions in the $Zn_{0.8}Cd_{0.2}S$ hollow spheres. The experimental results confirmed that Ni doping reduced the band structure of the substrate, suppressed the recombination of photo-induced electrons and holes, and provided more reactive sites. Therefore, the photocatalytic activity had been greatly improved. As a consequence, the detected photocatalytic H_2 evolution rate increased up to 33.81 mmol·h^{-1}·g^{-1} over an optimal Ni doping (5 wt %) of $Zn_{0.8}Cd_{0.2}S$ hollow spheres, which was 20.87-fold higher than that of pure CdS. Elemental mapping showed that the Zn element was mainly distributed in the outermost layer of the hollow spheres; this might be the critical factor that enabled Ni-doped $Zn_xCd_{1-x}S$ to maintain excellent stability.

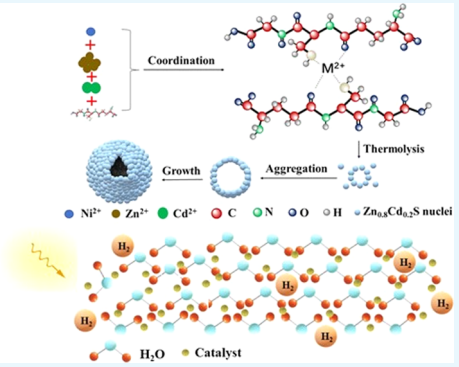

1. INTRODUCTION

Environmental problems and energy crisis are becoming increasingly more severe; therefore, it is imperative to discover novel, renewable, and environmentally friendly energy sources.[1] In 1972, Fujishima and Honda discovered that TiO_2 can be excited by ultraviolet light to produce H_2,[2] and hydrogen is clean energy with high energy density, which can greatly alleviate dependence on fossil fuels.[3] Therefore, research on converting solar energy into chemical energy to reduce water to generate H_2 has drawn immense attention.[4,5] Materials suitable for semiconductor photocatalytic H_2 evolution from water splitting must satisfy several conditions: they have a suitable band gap and suitable redox potential and meet the thermodynamic requirements.[6]

Over the past few years, a multitude of semiconductor materials that could fulfill the requirements of the hydrogen evolution reaction (HER) have been extensively developed, such as oxides (TiO_2), sulfides (CdS-based[7]), oxynitrides (TaON[8]), metal-free materials (g-C_3N_4[9,10]), etc. Unfortunately, hardly any single material can meet all of the requirements of photocatalytic hydrogen production, and there are always various defects, such as a wide band gap,[11] narrower corresponding range of light, responsiveness only to ultraviolet light,[12] the fast recombination speed of photo-generated carriers,[13] or the need for noble metals as cocatalysts.[14]

To solve the above problems, a lot of research has been carried out. Taking a classical CdS catalyst as an example, the CdS band structure is 2.40 eV, with a wider corresponding range of light,[15] and is widely explored as a good substrate material to composite with other materials.[16,17] However, CdS has some limitations; it is unstable during the reaction and is prone to undergo photocorrosion, with poor reusability.[18] In comparison with CdS, ZnS has better stability, but it can absorb light only in the ultraviolet region. Based on this feature, many researchers have complexed zinc sulfide and cadmium sulfide to establish a hybrid structure with improved hydrogen production activity and enhanced stability. For the combination of these two components into an effectively integrated catalyst system, various forms have been explored. For example, Wang et al., via a facile self-assembly route, synthesized ZnS−CdS alloys, used for degradation of rhodamine B.[19] Xie et al. synthesized a ZnS−CdS core−shell structure via a one-step solvothermal method to generate H_2, at a rate up to 792 μmol·h^{-1}·g^{-1}.[20] Zhang et al. used hydrothermally synthesized Zn−Cd−S solid solutions, with which the hydrogen evolution could reach 11.42 mmol·h^{-1}·g^{-1}.[21] Compared with other composite types, the $Zn_xCd_{1-x}S$ solid solution has unique advantages.[22−24]

As reported in the literature, CdS has various morphologies, such as nanofibers,[25] nanoplates,[26,27] nanowires,[28] nanorods,[29]

Received: December 11, 2020
Accepted: March 9, 2021
Published: May 21, 2021

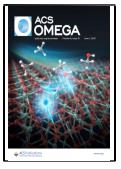

etc.; thus, numerous studies have been devoted to the influence of morphology and structure on activity. In addition to the above-mentioned strategy, the introduction of cocatalysts is also a universally used method to increase photocatalytic activity. In 1983, Nakabayashi et al. supported a Pt cocatalyst on TiO_2 as the active site for hydrogen production,[30] improved the photocatalytic hydrogen production activity, and opened a new era of cocatalysts. The Fermi level of a semiconductor photocatalyst is higher than the Fermi level of noble metals, and thus electrons migrate from the semiconductor to the metal and an excess negative charge will be created on the metal surface, forming a metal−hydrogen bond with hydrogen atoms, thereby boosting the photocatalytic performance by delaying the electron and hole pair recombination.[31] The generally used noble-metal promoters are Pd,[7] Pt,[26] Au,[32,33] Ag,[34] etc. However, because of their scarcity and high price, noble metals are not suitable for practical application. Research has found that the noble-metal-free Ni metal can also improve photocatalytic activity.[23,35,36] Various methods have been introduced for synthesizing cocatalysts, such as the MOF template method, the photodeposition method, the hydrothermal method, and so on.

Herein, a noble-metal-free Ni-doped $Zn_xCd_{1-x}S$ hollow sphere catalyst was successfully synthesized via a facile one-step hydrothermal method. We first explored the optimized ratio of Zn and Cd in $Zn_xCd_{1-x}S$ (x = 0, 0.20, 0.50, 0.80, 1) and determined that $Zn_{0.8}Cd_{0.2}S$ (denoted ZCS) had the optimal photocatalytic H_2 generation activity (7.25 mmol·h^{-1}·g^{-1}). After further modification by Ni doping (5 wt %), the hydrogen generation rate of ZCS reached up to 33.81 mmol·h^{-1}·g^{-1}, which is also 4.66 times and 20.87 times higher than those of ZCS and pure CdS, respectively. Combined with the experimental results, we proposed a possible photo-induced catalytic mechanism for Ni-doped $Zn_xCd_{1-x}S$.

2. RESULTS AND DISCUSSION

2.1. Phase Purity and Crystallographic Structure Analysis. The phase purity and crystallographic structure of the samples were examined by powder X-ray diffraction (XRD) analysis. As depicted in Figure 1, the characteristic peaks of all samples can be well assigned to the standard diffraction diagrams of CdS (JCPDS Card No. 47-1179) and ZnS (JCPDS Card No. 65-0309). It could be clearly seen that all samples had a peak that was slightly shifted to a large angle relative to the standard card. According to the previously reported literature, the ionic radius of Cd^{2+} (0.97 Å) is larger than that of Zn^{2+} (0.74 Å). This thus implies the doping of Zn^{2+} into the lattice of CdS, which reduced the distance between the stripes of CdS, indicating that we synthesized a ZCS solid solution.[21] With the introduction of Ni ions, the diffraction peak positions of all samples were consistent; the characteristic peaks of Ni were not observed. This may be ascribed to the high dispersion and the low content of the introduced Ni, which did not affect the morphology and structure of the ZCS sample, indicating that the improved catalyst activity is not mainly caused by the changes in morphology and structure but by the introduced Ni ions.[37] To explore the reason why Ni ions were not detected, we further examined 50 wt % Ni-doped ZCS (denoted ZCS-50) using powder X-ray diffraction (XRD) analysis, whose results also did not exhibit the diffraction peaks of nickel species (Figure S1), possibly because Ni ions were highly dispersed throughout the ZCS hollow sphere.[38−40]

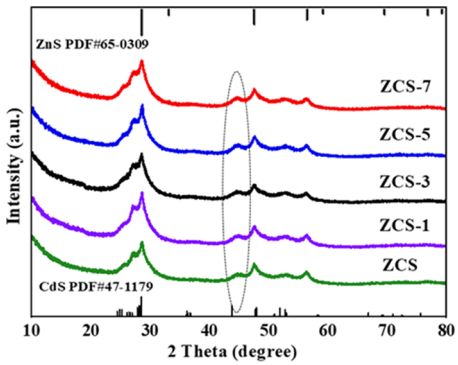

Figure 1. XRD patterns of the samples $Zn_{0.8}Cd_{0.2}S$, 1 wt % Ni-doped $Zn_{0.8}Cd_{0.2}S$, 3 wt % Ni-doped $Zn_{0.8}Cd_{0.2}S$, 5 wt % Ni-doped $Zn_{0.8}Cd_{0.2}S$, and 7 wt % Ni-doped $Zn_{0.8}Cd_{0.2}S$.

2.2. Morphologies and Elemental Distribution of Samples. Field emission scanning electron microscopy (FESEM) was used to reveal the morphologies of samples. As shown in Figure S2, the morphology of all samples showed a uniform spherical structure by disordered agglomerated nanoparticles. There was no visible change in morphology when Ni ions were introduced. The structural details of the ZCS-5 sample were obtained by transmission electron microscopy (TEM). As shown in Figure 2a, a spherelike nanostructure was observed and the color of the outermost layer of the nanosphere was found to be lighter, probably due to the lack of compaction in the surface. The middle layer was darker, and the innermost layer was lighter; this indicated the hollow structure of the nanosphere, as well as that the spherical structure consisted of particles. The morphology of the samples was further verified by the SEM images, as shown in Figure S2. Based on the HRTEM images in Figure 2b, we also measured the lattice fringes (0.21 nm) and compared with the standard card (JCPDS Card No. 47-1179); it corresponds to the (107) plane of CdS. The elemental mapping was applied in this work to probe the elemental distribution of the ZCS-5 nanosphere. In Figures 3a−e and S3, the nanosphere clearly exhibited Zn, Cd, S, and Ni, in line with the elemental composition of ZCS-5. More importantly, the introduced Ni was also clearly observed and was found to be highly distributed throughout the hollow spherical structure, indicating the successful doping of Ni with high dispersion in the ZCS nanosphere. From Figure 3e, we also clearly noticed that the Zn element was mainly scattered in the outermost layer; this might be the critical factor that enabled Ni-doped $Zn_xCd_{1-x}S$ to maintain excellent stability. We also measured the surface area of samples ZCS and ZCS-5 (Figure S4); the surface areas of samples ZCS and ZCS-5 were 87.09 and 39.52 m^2·g^{-1}, respectively.

2.3. Analysis of Surface Element Valence. X-ray photoelectron spectroscopy (XPS) was subsequently carried out to analyze the surface elements and chemical states of the ZCS nanosphere. Figure 4a shows that S, Zn, and Cd elements are present in the ZCS-5 sample. Taking the C 1s peak at 284.50 eV as the reference to calibrate binding energy (BE),[41] as depicted in Figure 4a, we did not discover the presence of Ni ions; this may be because of the low content of Ni and its high distribution throughout the hollow spherical structure, which thus results in a relatively low concentration on the surface that cannot reach the detection limit of XPS. To

https://doi.org/10.1021/acsomega.0c06038
ACS Omega 2021, 6, 13544−13553

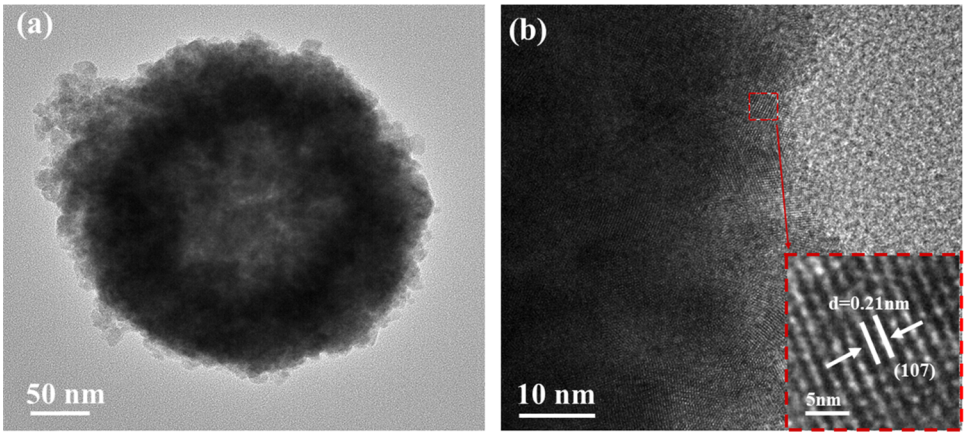

Figure 2. (a) TEM and (b) HRTEM images of 5 wt % Ni-doped $Zn_{0.8}Cd_{0.2}S$.

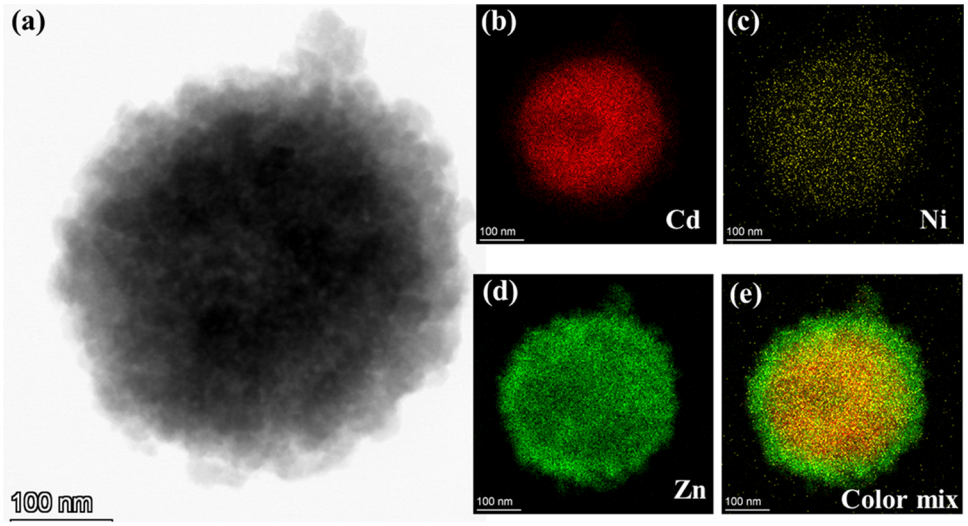

Figure 3. (a) Elemental mapping image of the 5 wt % Ni-doped $Zn_{0.8}Cd_{0.2}S$ sample, (b–d) corresponding elemental analysis, and (e) color mix.

confirm this speculation, we performed XPS testing on ZCS-50 samples. From Figure S5e, we found a satellite peak at 855.72 eV, which could be ascribed to the typical XPS signal of Ni $2p_{3/2}$, indicating the presence of +2 valence Ni.[17,42] Thus, the absence of Ni in the XPS result of the prepared ZCS-5 sample can be attributed to its relatively low content. After all, the Ni content on the surface of the ZCS-50 sample was only 0.30% (Table S1). Figure 4b shows that the band can be deconvolved into two peaks at 162.59 and 161.28 eV, which can be ascribed to the S $2p_{1/2}$ and S $2p_{3/2}$ tracks, respectively. This indicates the −2 valence of the S element in this system.[43] Besides, two peaks (Figure 4c) with binding energies of 1045.85 and 1022.83 eV can be attributed to Zn $2p_{1/2}$ and Zn $2p_{3/2}$, respectively, implying that the valence state of the Zn element was +2.[44] It could be evidently seen in Figure 4b–d that the peaks of S, Zn, and Cd were slightly shifted in the direction of higher binding energy (BE) levels. According to the literature, when metal ions are doped into a semiconductor, the Fermi level shifts in a more negative direction.[31,45,46] Therefore, Ni doping resulted in a peak shift, despite the fact that the Ni metal content on the surface of the hollow sphere was extremely low. The binding energy of Cd in ZCS of 411.62 eV corresponds to Cd $3d_{5/2}$ and 404.89 eV is ascribed to $3d_{3/2}$, which showed that Cd had +2 valence in this system.[10,44] Through the above analysis, we realized that in the Ni-doped ZCS system, Zn had +2 valence, Cd had +2 valence, Ni had +2 valence, and S had −2 valence. According to the above analysis, we proved that the Ni-doped ZCS hollow spheres were successfully synthesized.[36,41] To investigate the specific amount of the Ni element in the ZCS-5 sample, inductively coupled plasma atomic emission spectrometry (ICP-AES) was applied in this work (Table S2). By calculation, it was found that while adding 5 wt % $Ni(NO_3)_2{\cdot}6H_2O$ (nickel nitrate hexahydrate) in the system, at the same time, 0.06% of Ni ions were introduced into the hollow spheres.

2.4. Synthesis Mechanism. During the synthesis process, the glutathione (GSH) biomolecule was chosen as a sulfur source, according to a previous report in the literature, which contains −SH, with a strong bondability on metal ions.[47] Based on the experiment, the related literature was explored, and the possible mechanism of Ni-doped ZCS hollow sphere synthesis was proposed (Figure 5). First, the metal ions coordinated with GSH to form an ion complex. It then underwent high-temperature decomposition to form sulfide nuclei. At high temperatures, GSH decomposed to produce CO_2 and NH_3 bubbles. While these bubbles moved automatically, they also provided the center for sulfide self-assembly. With the continuous aggregation of sulfide particles, a densely packed spherical shell structure was gradually formed, and finally, a hollow spherical structure was formed.

https://doi.org/10.1021/acsomega.0c06038
ACS Omega 2021, 6, 13544−13553

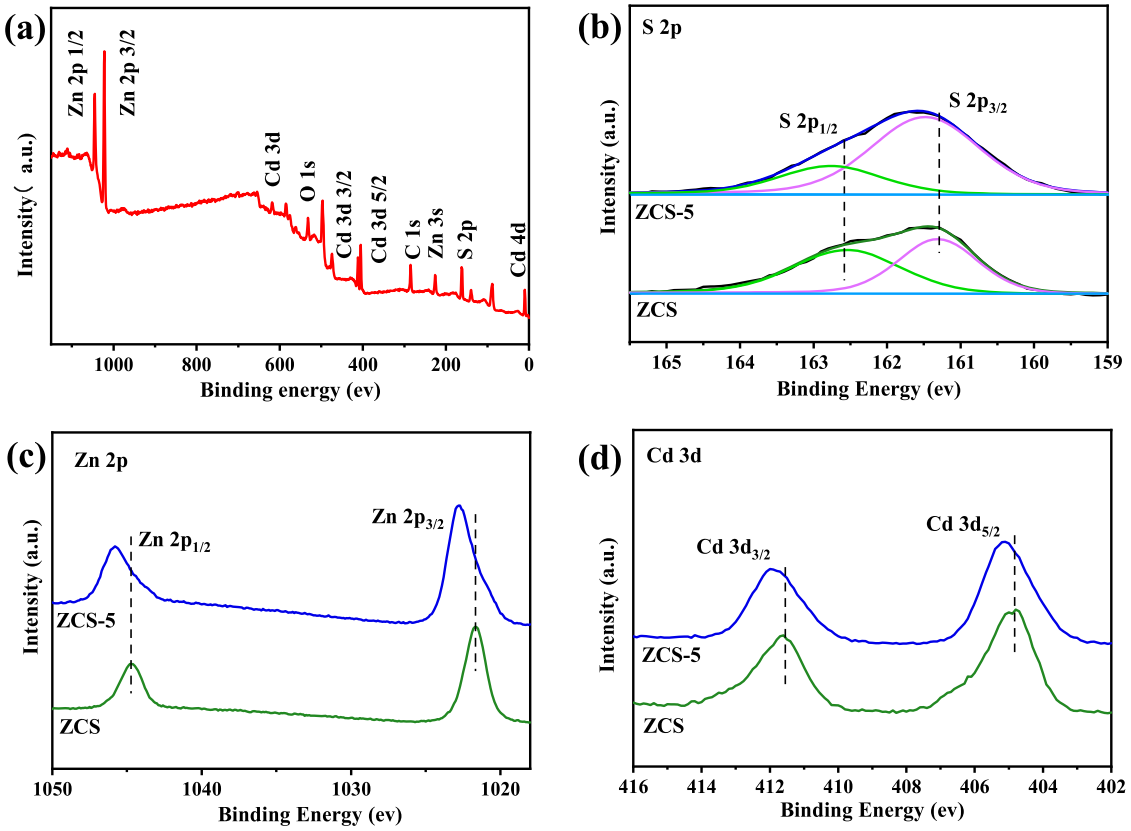

Figure 4. High-resolution XPS spectra of 5 wt % Ni-doped $Zn_{0.8}Cd_{0.2}S$ and $Zn_{0.8}Cd_{0.2}S$: (a) survey spectrum, (b) S 2p, (c) Zn 3d, and (d) Cd 2p.

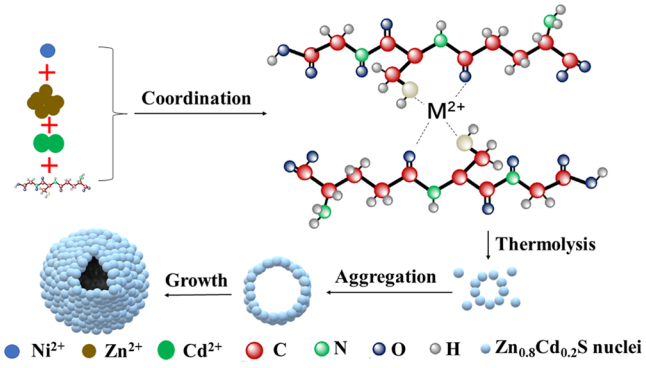

Figure 5. Schematic diagram of the synthesis route of Ni-doped $Zn_xCd_{1-x}S$.

2.5. Performance Testing. The photocatalytic performance of various Ni-doped ZCS samples was confirmed by a water-splitting hydrogen evolution measurement under visible light (λ > 420 nm), as depicted in Figure 6. The test time was 3 h, and the produced gas was monitored every 30 min (Figure 6a). In Figure S6, we can see that the H_2 generation rate of CdS was 1.62 mmol·h^{-1}·g^{-1}, and the activity of ZnS was 0.03 mmol·h^{-1}·g^{-1}. When Zn/Cd was 0.80:0.20, the catalyst activity was measured to be the highest, and the rate of hydrogen production was 7.25 mmol·h^{-1}·g^{-1}, which was 4.48 times higher than that of CdS. Moreover, when Ni ions were introduced into the system, the catalytic activity of the whole system could be further enhanced. When the doping amount of Ni ions reached 5 wt %, the photocatalytic water-splitting hydrogen generation activity of the reaction system was optimal, up to 33.81 mmol·h^{-1}·g^{-1}, which was 4.66 times higher than that of ZCS. It was worth noting that when the content of Ni reached 7 wt %, the H_2 generation capacity dropped instead, possibly because excessive Ni ions serve as charge recombination centers.[22] On the other hand, we also confirmed by an experiment that the sacrificial agent in the system (0.35 M $Na_2S·9H_2O$ and 0.25 M Na_2SO_3) did not produce hydrogen under visible light, excluding the potential extra influence of the sacrificial agent.

In the four cycles, the sacrificial reagents chosen were still 0.35 M $Na_2S·9H_2O$ and 0.25 M Na_2SO_3 and every cycle was maintained for 3 h. From Figure 6c, we observed that after four cycles, the hydrogen production rate was still 28.90 mmol·h^{-1}·g^{-1}, indicating that the catalyst was stable. The XRD and SEM images shown in Figure 6d and XRD diffraction peaks were consistent with those before the reaction, implying that the crystal form of the sample does not vary after four cycles, and the surface morphology remained unchanged. However, the photocatalytic water-splitting hydrogen generation rate declined a little; this was also in line with the fact that sulfides are prone to photocorrosion under light irradiation.

2.6. Optical Properties. Light absorption characteristics of samples were examined by UV−visible diffuse reflectance spectra (DRS). Figure 7a reveals that all catalysts had a strong visible light absorption ability, but the light response curve of all samples was almost unchanged. The intuitive image of samples shows, as expected, that the color did not change. The optical band gap energies were calculated by the Kubelka−Munk equation. By calculation, the ZCS-5 sample band gap was found to be 2.62 eV, slightly smaller than that of pure ZCS (2.63 eV). A Mott−Schottky measurement was conducted on samples ZCS and ZCS-5. Both ZCS and ZCS-5 samples have positive slopes, so they are n-type semiconductors. The flat

https://doi.org/10.1021/acsomega.0c06038
ACS Omega 2021, 6, 13544−13553

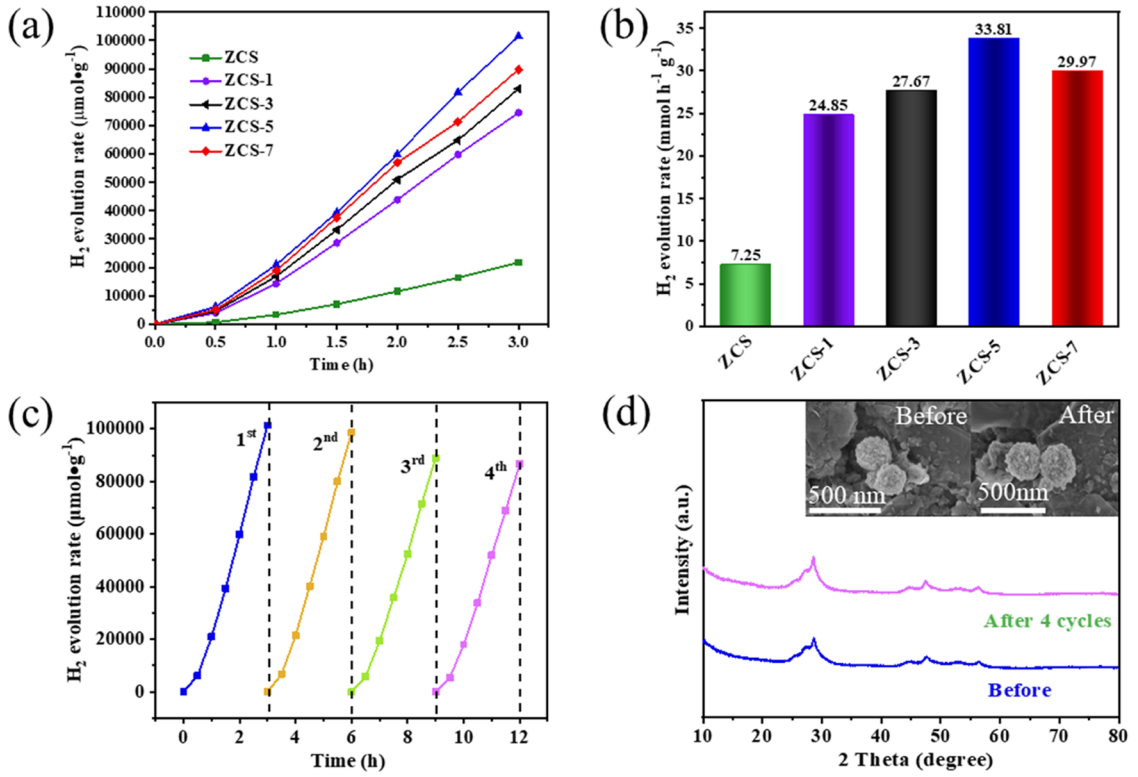

Figure 6. (a) Time course of H_2 evolution of the samples, (b) H_2 evolution rate of the samples, (c) recycling experiments over the 5 wt % Ni-doped $Zn_{0.8}Cd_{0.2}S$ sample, and (d) XRD patterns and SEM images of the 5 wt % Ni-doped $Zn_{0.8}Cd_{0.2}S$ sample after four cycles.

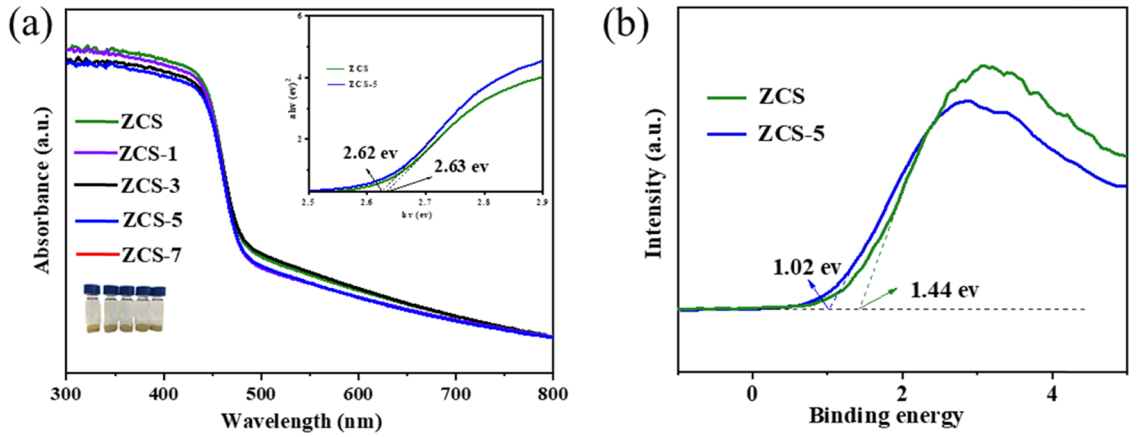

Figure 7. (a) DRS spectra of the samples and (b) XPS valence band spectra of $Zn_{0.8}Cd_{0.2}S$ and 5 wt % Ni-doped $Zn_{0.8}Cd_{0.2}S$.

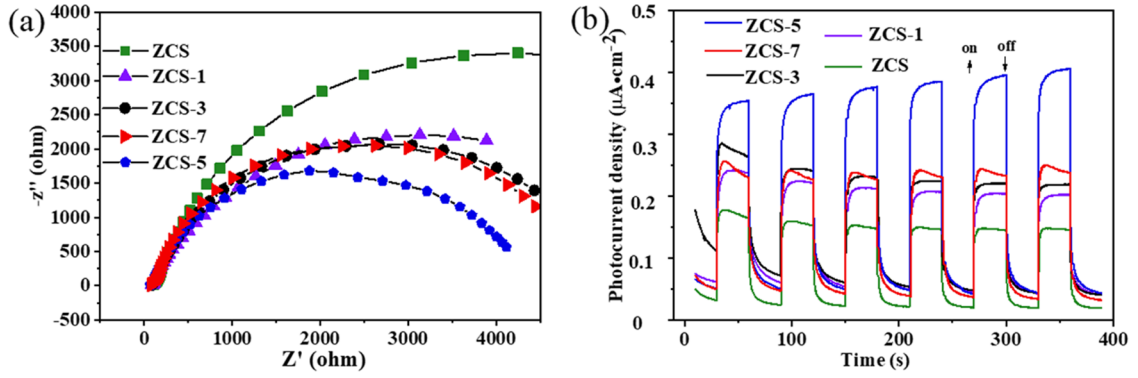

Figure 8. (a) Impedance tests and (b) transient photocurrent of all of the samples.

https://doi.org/10.1021/acsomega.0c06038
ACS Omega 2021, 6, 13544−13553

band potential (E_{fb}) of ZCS was −1.04 V and that of ZCS-5 was −1.42 V; according to the literature,[6] the n-type semiconductor conduction band potential (E_{CB}) is more negative by 0.1 or 0.2 V as compared to the corresponding E_{fb} (Figure S6). For the purpose of further explaining the reasons for the change in photocatalytic activity, we performed valence band XPS measurements on the ZCS and ZCS-5 samples. The valence band values of samples ZCS and ZCS-5 were 1.44 and 1.02 eV (Figure 7b), respectively. Combined with the calculation of the band gap, we concluded that the conduction band value of sample ZCS-5 was −1.60 eV, more negative than that of sample ZCS (−1.19 eV). The conduction band value was more negative and more suitable for hydrogen production.[48,49] We performed a PL measurement to ascertain the separation efficiency of photogenerated carriers. The ZCS sample has the fastest photogenerated carrier recombination rate, and the ZCS-5 sample has the slowest photogenerated carrier recombination rate (Figure S7).

As we know, the separation efficiency of photogenerated carriers has a great influence on catalytic activity.[50] To further interpret the reason for the improved activity of the system after the introduction of Ni ions, we performed impedance tests and transient photocurrent response tests. As can be seen from Figure 8a, pure ZCS showed the highest impedance intensity and ZCS-5 presented the lowest impedance intensity. It was suggested that in the photo-induced process of charge-carrier transfer, the resistance encountered in the ZCS system was smaller, more conducive to the enhanced activity of carrier transfer, thus suggesting the reason for the enhanced activity of the ZCS-5 system. Photocurrent measurements showed the same trend. From Figure 8b, it is clear that the ZCS-5 sample had the strongest light response and pure-phase ZCS had the weakest light response intensity, indicating that the ZCS-5 sample had the highest charge separation and migration efficiency among other concentrations of Ni-modified samples.[51]

On the basis of the above discussion, a possible photocatalytic hydrogen evolution mechanism for the Ni-doped ZCS catalyst is illustrated in Figure 9. When the incident light

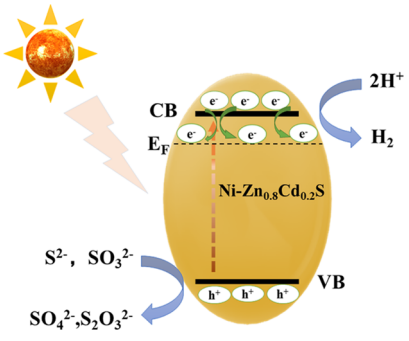

Figure 9. Mechanism of photocatalytic H_2 production over Ni-doped $Zn_xCd_{1-x}S$ under visible light irradiation.

energy is greater than the semiconductor band gap, the valence electrons enable the valence band to gain energy and transfer it to the conductor, leaving holes in the valence band. Ni-doped ZCS was excited under light irradiation to generate electrons, and the inherent conduction band minimum (CBM) of ZCS-5 (−1.60 eV), which has a more negative potential than the H^+/H_2 energy level, ensures that the photogenerated electrons have a capability to proceed with the hydrogen evolution reaction. On the other hand, the photogenerated holes were immediately captured by the sacrificial agent (Na_2S/Na_2SO_3) during the reaction, so that the continuously produced electrons can successfully drive hydrogen generation. When Ni ions were introduced into the system, they possibly coordinated with GSH to form NiS; the potential of Ni^{2+}/Ni was approximately −0.23 V (vs standard hydrogen electrode (SHE), pH = 0), lower than the conduction band position of ZCS. The electrons generated by light excitation can be transferred to nickel sulfide after transitioning to the conduction band of ZCS to effectively separate the photogenerated electrons and holes. More importantly, the introduced Ni ions with high dispersion throughout the structure not only provide reactive sites for the electrons to react with H^+ in water but also effectively improve the charge transfer of electrons, thus promoting the charge-carrier-involved hydrogen evolution in photocatalysis.[52,53]

3. CONCLUSIONS

In summary, we synthesized Ni-doped ZCS hollow sphere photocatalysts through a facile one-step hydrothermal method. The ZCS-5 sample exhibited superior photocatalytic performance. The H_2 evolution rate could reach 33.81 $mmol \cdot h^{-1} \cdot g^{-1}$, which was 20.87 times higher than that of pure CdS and was also higher than that of the noble-metal-free sulfide catalyst (Table 1). Moreover, the established system demonstrated excellent stability in the cycle test. Through a series of characterizations, the significant improvement of photocatalytic performance can be chiefly ascribed to the high dispersion of the doped Ni throughout the structure, which not only provides active sites for the photogenerated electrons but also effectively improves the charge-carrier transfer. We hope that this work will provide some hints for the synthesis of highly active CdS-based catalysts.

4. EXPERIMENTAL SECTION

4.1. Materials. $Zn(NO_3)_2 \cdot 6H_2O$, $Cd(NO_3)_2 \cdot 4H_2O$, $Ni(NO_3)_2 \cdot 6H_2O$, Na_2SO_3, and $Na_2S \cdot 9H_2O$ were provided by Sinopharm Chemical Reagent Co., Ltd. (Shanghai, China), and glutathione was purchased from Aladdin, which was of analytical grade and directly used without further processing. Double-distilled water was used in the experiment.

4.2. Synthesis of Ni-Doped ZCS Hollow Sphere Catalysts. *4.2.1. Synthesis of the $Zn_xCd_{1-x}S$ Catalyst.* ZCS hollow sphere catalysts were synthesized using a one-step solvothermal synthesis method. To probe the optimal ratio of Zn and Cd, we synthesized a series of catalysts with different Zn^{2+} and Cd^{2+} ratios; with x values of 0, 0.20, 0.50, 0.80, and 1.00; $Zn^{2+} + Cd^{2+}$ = 1.60 mmol; and $(Zn^{2+} + Cd^{2+})/S$ = 1:1. Then, x mmol of $Zn(NO_3)_2 \cdot 6H_2O$ (zinc nitrate hexahydrate), $(1.6 - x)$ mmol of $Cd(NO_3)_2 \cdot 4H_2O$, and 1.6 mmol of glutathione were dissolved separately in 30 mL of double-distilled water. The resulting mixed solution was subjected to ultrasound for 10 min, and then stirring was continued for 30 min. After complete dissolution, a white solution was obtained, which was then transferred to a 100 mL Teflon-lined autoclave and hydrothermally treated at 140 °C, maintained for 24 h. After the reaction was completed, the autoclave was cooled naturally to room temperature. The obtained yellow solution was collected by centrifugation, washed with deionized water and ethanol several times, and vacuum-dried at 60 °C overnight.

https://doi.org/10.1021/acsomega.0c06038
ACS Omega 2021, 6, 13544−13553

Table 1. List of Photocatalytic Activities of Similar Catalysts

catalyst	synthesis method	light source	sacrificial agent	H_2 generation ($mmol \cdot h^{-1} \cdot g^{-1}$)	ref
5 wt % Ni-doped $Zn_{0.8}Cd_{0.2}S$	one-step hydrothermal method	300 W Xe lamp ($\lambda \geq 420$ nm cutoff filter)	0.35 M Na_2S and 0.25 M Na_2SO_3	33.81	here
$NiS/Zn_xCd_{1-x}S$	MOF template	300 W Xe lamp ($\lambda > 420$ nm cutoff filter)	0.35 M Na_2S and 0.25 M Na_2SO_3	16.78	35
$Pt/Zn_xCd_{1-x}S$	several-step hydrothermal method	300 W Xe lamp ($\lambda > 420$ nm cutoff filter)	lactic acid	4.11	54
$Zn_{0.64}Cd_{0.36}S$	second-growth method	300 W Xe lamp ($\lambda > 420$ nm cutoff filter)	0.35 M Na_2S and 0.25 M Na_2SO_3	0.815	55
CdS-MOF	MOF template method	300 W Xe lamp ($\lambda > 380$ nm cutoff filter)	27:3 CH_3CN/lactic acid	1.725	56
$MoS_2(5\%)/Zn_{0.5}Cd_{0.5}S/g\text{-}C_3N_4(30\%)$	several-step hydrothermal method distillation calcination	300 W Xe lamp ($\lambda \geq 400$ nm cutoff filter)	0.35 M Na_2S and 0.25 M Na_2SO_3	4.914	57
$Ni_2P-Zn_{0.5}Cd_{0.5}S$	one-step hydrothermal method	300 W Xe lamp ($\lambda \geq 420$ nm cutoff filter)	0.35 M Na_2S and 0.25 M Na_2SO_3	0.912	58
β-$Ni(OH)_2$-CdS	template, deposition method	300 W Xe lamp ($\lambda \geq 420$ nm cutoff filter)	ethanol (10 vol %)	1.4	15
$Zn_{0.8}Cd_{0.2}S@g\text{-}C_3N_4$-10 wt %	calcination, hydrothermal method	300 W Xe lamp ($\lambda \geq 420$ nm cutoff filter)	0.35 M Na_2S and 0.25 M Na_2SO_3	2.35	59
$Ni_xB-Zn_xCd_{1-x}S$	hydrothermal, redox method	5 W Xe lamp	lactic acid	1.52	23
$NiCo_2S_4@Zn_{0.5}Cd_{0.5}S$	several-step hydrothermal method	Xe lamp ($\lambda > 420$ nm cutoff filter)	0.02 M PTA and 0.1 M NaOH	0.233	60

4.2.2. Synthesis of the Ni-Doped ZCS Catalyst. Different amounts of $Ni(NO_3)_2 \cdot 6H_2O$ (nickel nitrate hexahydrate, 0, 1, 3, 5, and 7 wt %) were added into the above solution before sonicating; the follow-up operations were the same, and the obtained samples were denoted ZCS, ZCS-1, ZCS-3, ZCS-5, and ZCS-7, respectively.

4.3. Characterization. The crystal structure of the samples was analyzed by X-ray diffraction (XRD) (Cu Kα = 1.5404 Å) (Bruker D8 Advance, Germany) at a scan rate of 0.05°/s and a 2θ range of 10−80°. The sample's surface morphology was observed with an SU8010 field emission scanning electron microscope (FESEM, Hitachi, Hitachi) under a deceleration voltage of 1.50 kV. Transmission electron microscopy (TEM) and high-resolution transmission electron microscopy (HRTEM) were performed in an accelerating mode of 200 kV (JEOL 2100-F). The energy-dispersive spectrum (EDS) was an attachment to HRTEM. The sample's surface elemental composition and chemical valence were characterized by VG Multi-lab 2000 (VG) X-ray photoelectron spectroscopy (XPS). The C 1s peak binding energy (284.50 eV) of surface-adsorbed carbon was used as the calibration standard. The specific element content was detected by inductively coupled plasma atomic emission spectrometry (ICP-AES) (Agilent, 700 series 730). UV−visible solid diffuse reflectance (DRS) was tested on an Agilent Cary-5000 spectrophotometer. In the UV−vis diffuse reflection experiments, $BaSO_4$ was used as the reference material, and the spectral scan range was 200−800 nm.

4.4. Photocatalytic Performance. Photocatalytic hydrogen production was used to evaluate catalytic activity. The HER experiments were carried out under a 300 W Xe lamp (Perfectlight PLS-SXE300) combined with an optical cutoff filter, with $\lambda > 420$ nm, at a fixed distance (10 cm). The average intensity of irradiation was measured as 13.80 $mW \cdot cm^{-2}$ (FZ-A spectroradiometer), and the irradiation area was 38.47 cm^2; the reactor was a top-irradiation-type Pyrex reaction cell attached to a closed gas evacuation and circulation system (equipped with perpetual cooling water). The specific process is as follows: 20 mg of catalyst was dispersed in 100 mL of aqueous solution containing $Na_2S \cdot 9H_2O$ (0.35 M, 8.4 g) and Na_2SO_3 (0.25 M, 3.15 g) as the hole scavengers; then, the mixed solution was subjected to ultrasonic vibration for 30 min, and a light-yellow uniform aqueous solution was obtained. Afterward, the reaction system was carefully sealed before nitrogen (the gas chromatography carrier gas was nitrogen) evacuation for 60 min to completely remove air. The reaction was performed at intervals of 0.50 h, and 400 μL of the sample of gas was taken from the reactor under constant magnetic stirring. A gas chromatograph (Fuli 9790) with a 5 Å molecular sieve column was used to analyze the hydrogen content. The specific concentration was quantitatively analyzed by a hydrogen standard curve.

4.5. Photoelectrochemical Measurements. Electrochemical impedance spectroscopy (EIS) and photocurrent−time curves were recorded on a Princeton electrochemical workstation (CHI-760E). As a counter electrode, we selected a platinum electrode, and a Ag/AgCl electrode was used as the reference electrode; the working electrodes were prepared as follows: 10 mg of the sample was dispersed in 1 mL of ethanol solution; then, 150 μL of Nafion was added to the above solution and subjected to ultrasound treatment for 30 min. Then, 5 drops of the dispersion solution were uniformly coated on the surface of F-doped tin oxide (FTO) (1 cm × 1 cm) and dried in infrared light using GUV-310 420 nm lamps as the

https://doi.org/10.1021/acsomega.0c06038
ACS Omega 2021, 6, 13544−13553

light source, and 0.50 M Na_2SO_4 was used as the electrolyte solution. Electrochemical impedance spectroscopy (EIS) measurements were performed at an amplitude of 5 mV, quiet time of 2 s, and a frequency range of $1-10^5$ Hz with the initial potential (1.50 V). The tests were performed at 5 mV of alternating current signal, and the data obtained were fitted using ZSimpWin software.

■ ASSOCIATED CONTENT

Supporting Information

The Supporting Information is available free of charge at https://pubs.acs.org/doi/10.1021/acsomega.0c06038.

(1) XRD patterns of the ZCS-5 and ZCS-50 samples; (2) SEM images of CdS, $Zn_{0.8}Cd_{0.2}S$, 1 wt % Ni-doped $Zn_{0.8}Cd_{0.2}S$, 3 wt % Ni-doped $Zn_{0.8}Cd_{0.2}S$, 5 wt % Ni-doped $Zn_{0.8}Cd_{0.2}S$, and 7 wt % Ni-doped $Zn_{0.8}Cd_{0.2}S$; (3) elemental mapping image of the 5 wt % Ni-doped $Zn_{0.8}Cd_{0.2}S$ sample and the corresponding S elemental analysis; (4) N_2 adsorption−desorption isotherms; (5) high-resolution XPS spectra of the 50 wt % Ni-doped $Zn_{0.8}Cd_{0.2}S$ sample; (6) surface element content of the ZCS-50 sample; (7) analysis of the element content of the ZCS-5 sample; (8) time course of H_2 evolution and H_2 evolution rate of the samples; (9) Mott−Schottky curves of (a) ZCS and (b) ZCS-5; and (10) PL spectra of all of the samples (PDF)

■ AUTHOR INFORMATION

Corresponding Author

Juncheng Hu − *Hubei Key Laboratory of Catalysis and Materials Science, School of Chemistry and Materials Science, South-Central University for Nationalities, Wuhan 430074, China;* orcid.org/0000-0003-0896-1474; Phone: +86 27 67841302; Email: jchu@mail.scuec.edu.cn

Authors

Ying Luo − *Hubei Key Laboratory of Catalysis and Materials Science, School of Chemistry and Materials Science, South-Central University for Nationalities, Wuhan 430074, China*

Xiaohui Zhang − *Hubei Key Laboratory of Catalysis and Materials Science, School of Chemistry and Materials Science, South-Central University for Nationalities, Wuhan 430074, China*

Cheng Huang − *Hubei Key Laboratory of Catalysis and Materials Science, School of Chemistry and Materials Science, South-Central University for Nationalities, Wuhan 430074, China*

Xiaole Han − *Hubei Key Laboratory of Catalysis and Materials Science, School of Chemistry and Materials Science, South-Central University for Nationalities, Wuhan 430074, China*

Qingqing Jiang − *Hubei Key Laboratory of Catalysis and Materials Science, School of Chemistry and Materials Science, South-Central University for Nationalities, Wuhan 430074, China*

Tengfei Zhou − *Institutes of Physical Science and Information Technology, Anhui University, Hefei 230601, China; Institute for Superconducting & Electronic Materials, School of Mechanical, Materials, Mechatronics & Biomedical Engineering, Faculty of Engineering and Information Sciences, University of Wollongong, Wollongong 2500, NSW, Australia;* orcid.org/0000-0002-7364-0434

Haijian Yang − *Hubei Key Laboratory of Catalysis and Materials Science, School of Chemistry and Materials Science, South-Central University for Nationalities, Wuhan 430074, China;* orcid.org/0000-0001-9644-6207

Complete contact information is available at: https://pubs.acs.org/10.1021/acsomega.0c06038

Notes

The authors declare no competing financial interest.

■ ACKNOWLEDGMENTS

This work was supported by the National Natural Science Foundation of China (21673300) and the Fundamental Research Funds for the Central Universities (CZT19001).

■ REFERENCES

(1) Walter, M. G.; Emliy, L. W.; James, R. M.; Shannon, W. B.; Mi, Q.; Elizabeth, A. S.; Nathan, S. L. Solar water splitting cells. *Chem. Rev.* **2010**, *110*, 6446−6473.

(2) Fujishima, A.; Honda, K. Electrochemical Photolysis of Water at a Semiconductor Electrode. *Nature* **1972**, *238*, 37−38.

(3) Navarro, R. M.; Sánchez-Sánchez, M. C.; Alvarez-Galvan, M. C.; Valle, F.; Fierro, J. L. G. Hydrogen production from renewable sources: biomass and photocatalytic opportunities. *Energy Environ. Sci.* **2009**, *2*, 35−54.

(4) Yan, X.; Jin, Z.; Zhang, Y.; Zhang, Y.; Yuan, H. Sustainable and efficient hydrogen evolution over a noble metal-free WP double modified ZnxCd1-xS photocatalyst driven by visible-light. *Dalton Trans.* **2019**, *48*, 11122−11135.

(5) Zhu, C.; Liu, C.; Fu, Y.; Gao, J.; Huang, H.; Liu, Y.; Kang, Z. Construction of CDs/CdS photocatalysts for stable and efficient hydrogen production in water and seawater. *Appl. Catal., B* **2019**, *242*, 178−185.

(6) Navarro, R. M.; Alvarez-Galván, M. C.; Villoria de la Mano, J. A.; Al-Zahrani, S. M.; Fierro, J. L. G. A framework for visible-light water splitting. *Energy Environ. Sci.* **2010**, *3*, 1865−1882.

(7) Sun, Q.; Wang, N.; Yu, J.; Yu, J. C. A Hollow Porous CdS Photocatalyst. *Adv. Mater.* **2018**, *30*, No. 1804368.

(8) Ullah, H.; Tahir, A. A.; Bibi, S.; Mallick, T. K.; Karazhanov, S. Z. Electronic properties of β-TaON and its surfaces for solar water splitting. *Appl. Catal., B* **2018**, *229*, 24−31.

(9) Yao, L.; Wei, D.; Ni, Y.; Yan, D.; Hu, C. Surface localization of CdZnS quantum dots onto 2D g-C3N4 ultrathin microribbons: Highly efficient visible light-induced H2-generation. *Nano Energy* **2016**, *26*, 248−256.

(10) Liu, H.; Jin, Z.; Xu, Z. Hybridization of Cd0.2Zn0.8S with g-C3N4 nanosheets: a visible-light-driven photocatalyst for H2 evolution from water and degradation of organic pollutants. *Dalton Trans.* **2015**, *44*, 14368−14375.

(11) Wang, G.; Huang, B.; Li, Z.; Lou, Z.; Wang, Z.; Dai, Y.; Whangbo, M. H. Synthesis and characterization of ZnS with controlled amount of S vacancies for photocatalytic H2 production under visible light. *Sci. Rep.* **2015**, *5*, No. 8544.

(12) Schneider, J.; Matsuoka, M.; Takeuchi, M.; Zhang, J.; Horiuchi, Y.; Anpo, M.; Bahnemann, D. W. Understanding TiO2 photocatalysis: mechanisms and materials. *Chem. Rev.* **2014**, *114*, 9919−9986.

(13) Chen, H.; Sun, Z.; Ye, S.; Lu, D.; Du, P. Molecular cobalt−salen complexes as novel cocatalysts for highly efficient photocatalytic hydrogen production over a CdS nanorod photosensitizer under visible light. *J. Mater. Chem. A* **2015**, *3*, 15729−15737.

(14) Lingampalli, S. R.; Ujjal, K. G.; Rao, C. N. R. Highly efficient photocatalytic hydrogen generation by solution-processed ZnO/Pt/CdS, ZnO/Pt/Cd1-xZnxS and ZnO/Pt/CdS1-xSex hybrid nanostructures. *Energy Environ. Sci.* **2013**, *6*, 3589−3594.

(15) Vamvasakis, I.; Ioannis, I. P.; Theocharis, T.; Charalampos, D.; Choulis, S. A.; Stella, K.; Gerasimos, S. A. Visible-Light Photocatalytic

H2 Production Activity of β-Ni(OH)2-Modified CdS Mesoporous Nanoheterojunction Networks. *ACS Catal.* **2018**, *8*, 8726−8738.
(16) Kumar, D. P.; Song, M. I.; Hong, S.; Kim, E. H.; Gopannagari, M.; Reddy, D. A.; Tae, K. K. Optimization of Active Sites of MoS2 Nanosheets Using Nonmetal Doping and Exfoliation into Few Layers on CdS Nanorods for Enhanced Photocatalytic Hydrogen Production. *ACS Sustainable Chem. Eng.* **2017**, *5*, 7651−7658.
(17) Wang, J. J.; Wang, J.; Feng, K.; Zhang, H. H.; Li, Z. J.; Liu, B.; Tung, C. H.; Wu, L. Z. Enhanced visible-light-driven hydrogen generation by in situ formed photocatalyst RGO-CdS-NixS from metal salts and RGO-CdS composites. *J. Mater. Chem. A* **2017**, *5*, 9537−9543.
(18) Li, Q.; Guo, B.; Yu, J.; Ran, J.; Zhang, B.; Yan, H.; Gong, J. R. Highly efficient visible-light-driven photocatalytic hydrogen production of CdS-cluster-decorated graphene nanosheets. *J. Am. Chem. Soc.* **2011**, *133*, 10878−10884.
(19) Wang, W.; Zhu, W.; Xu, H. Monodisperse, Mesoporous ZnxCd1-xS Nanoparticles as Stable Visible-Light-Driven Photocatalysts. *J. Phys. Chem. C* **2008**, *112*, 16754−16758.
(20) Xie, Y. P.; Yu, Z. B.; Liu, G.; Ma, X. L.; Cheng, H.-M. CdS−mesoporous ZnS core−shell particles for efficient and stable photocatalytic hydrogen evolution under visible light. *Energy Environ. Sci.* **2014**, *7*, 1895−1901.
(21) Zhang, X.; Zhao, Z.; Zhang, W.; Zhang, G.; Qu, D.; Miao, X.; Sun, S.; Sun, Z. Surface Defects Enhanced Visible Light Photocatalytic H2 Production for Zn-Cd-S Solid Solution. *Small* **2016**, *12*, 793−801.
(22) Huang, D.; Wen, M.; Zhou, C.; Li, Z.; Cheng, M.; Chen, S.; Xue, W.; Lei, L.; Yang, Y.; Xiong, W.; Wang, W. ZnxCd1-xS based materials for photocatalytic hydrogen evolution, pollutants degradation and carbon dioxide reduction. *Appl. Catal., B* **2020**, *267*, No. 118651.
(23) Cao, Y.; Wang, G.; Ma, Q.; Jin, Z. An amorphous nickel boride-modified ZnxCd1-xS solid solution for enhanced photocatalytic hydrogen evolution. *Dalton Trans.* **2020**, *49*, 1220−1231.
(24) Chan, C.; Chang, C.; Hsu, C.; Weng, Y.; Chen, K.; Lin, H.; Huang, W.; Cheng, S. Efficient and stable photocatalytic hydrogen production from water splitting over ZnxCd1−xS solid solutions under visible light irradiation. *Int. J. Hydrogen Energy* **2014**, *39*, 1630−1639.
(25) Cheng, L.; Xiang, Q.; Liao, Y.; Zhang, H. CdS-Based photocatalysts. *Energy Environ. Sci.* **2018**, *11*, 1362−1391.
(26) Li, Q.; Zhao, F.; Qu, C.; Shang, Q.; Xu, Z.; Yu, L.; McBride, J. R.; Lian, T. Two-Dimensional Morphology Enhances Light-Driven H2 Generation Efficiency in CdS Nanoplatelet-Pt Heterostructures. *J. Am. Chem. Soc.* **2018**, *140*, 11726−11734.
(27) Deng, F.; Liu, X.; Luo, Y.; Wang, J.; Che, W.; Yang, R.; Luo, X.; Luo, S.; Dionysiou, D. D. Novel visible-light-driven direct Z-scheme CdS/CuInS2 nanoplates for excellent photocatalytic degradation performance and highly-efficient Cr(VI) reduction. *Chem. Eng. J.* **2019**, *361*, 1451−1461.
(28) Tang, Z.; Han, B.; Han, C.; Xu, Y. One dimensional CdS based materials for artificial photoredox reactions. *J. Mater. Chem. A* **2017**, *5*, 2387−2410.
(29) Simon, T.; Bouchonville, N.; Berr, M. J.; Vaneski, A.; Adrovic, A.; Volbers, D.; Wyrwich, R.; Doblinger, M.; Susha, A. S.; Rogach, A. L.; Jackel, F.; Stolarczyk, J. K.; Feldmann, J. Redox shuttle mechanism enhances photocatalytic H2 generation on Ni-decorated CdS nanorods. *Nat. Mater.* **2014**, *13*, 1013−1018.
(30) Nakabayashi, S.; Akira, F.; Kenichi, H. Experimental Evdence for The Hydrogen Evolution Site In Photocatalytic Process On Pt/TiO2. *Chem. Phys. Lett.* **1983**, *102*, 464−465.
(31) Subramanian, V.; Eduardo, E. W.; Prashant, V. K. Catalysis with TiO2/Gold Nanocomposites. Effect of Metal Particle Size on the Fermi Level Equilibration. *J. Am. Chem. Soc.* **2004**, *126*, 4943−4950.
(32) Naya, S. I.; Kume, T.; Akashi, R.; Fujishima, M.; Tada, H. Red-Light-Driven Water Splitting by Au(Core)-CdS(Shell) Half-Cut Nanoegg with Heteroepitaxial Junction. *J. Am. Chem. Soc.* **2018**, *140*, 1251−1254.
(33) Chen, Y.; Huang, Y.; Huang, H.; Su, P.; Perng, T.; Chen, L. Photocatalytic enhancement of hydrogen production in water splitting under simulated solar light by band gap engineering and localized surface plasmon resonance of ZnxCd1-xS nanowires decorated by Au nanoparticles. *Nano Energy* **2020**, *67*, No. 104225.
(34) Stroyuk, O.; Raevskaya, A.; Gaponik, N.; Selyshchev, O.; Dzhagan, V.; Schulze, S.; Zahn, D. R. T. Origin of the Broadband Photoluminescence of Pristine and Cu+/Ag+-Doped Ultrasmall CdS and CdSe/CdS Quantum Dots. *J. Phys. Chem. C* **2018**, *122*, 10267−10277.
(35) Zhao, X.; Feng, J.; Liu, J.; Shi, W.; Yang, G.; Wang, G. C.; Cheng, P. An Efficient, Visible-Light-Driven, Hydrogen Evolution Catalyst NiS/Znx Cd1-x S Nanocrystal Derived from a Metal-Organic Framework. *Angew. Chem., Int. Ed.* **2018**, *57*, 9790−9794.
(36) Dai, D.; Wang, L.; Xiao, N.; Li, S.; Xu, H.; Liu, S.; Xu, B.; Lv, D.; Gao, Y.; Song, W.; Ge, L.; Liu, J. In-situ synthesis of Ni2P co-catalyst decorated Zn0.5Cd0.5S nanorods for high-quantum-yield photocatalytic hydrogen production under visible light irradiation. *Appl. Catal., B* **2018**, *233*, 194−201.
(37) Ran, J.; Zhu, B.; Qiao, S. Z. Phosphorene Co-catalyst Advancing Highly Efficient Visible-Light Photocatalytic Hydrogen Production. *Angew. Chem., Int. Ed.* **2017**, *56*, 10373−10377.
(38) Liu, J.; Meeprasert, J.; Namuangruk, S.; Zha, K.; Li, H.; Huang, L.; Maitarad, P.; Shi, L.; Zhang, D. Facet−Activity Relationship of TiO2 in Fe2O3/TiO2 Nanocatalysts for Selective Catalytic Reduction of NO with NH3: In Situ DRIFTs and DFT Studies. *J. Phys. Chem. C* **2017**, *121*, 4970−4979.
(39) Liu, Y.; Ding, S.; Shi, Y.; Liu, X.; Wu, Z.; Jiang, Q.; Zhou, T.; Liu, N.; Hu, J. Construction of CdS/CoOx core-shell nanorods for efficient photocatalytic H2 evolution. *Appl. Catal., B* **2018**, *234*, 109−116.
(40) Han, J.; Meeprasert, J.; Maitarad, P.; Nammuangruk, S.; Shi, L.; Zhang, D. Investigation of the Facet-Dependent Catalytic Performance of Fe2O3/CeO2 for the Selective Catalytic Reduction of NO with NH3. *J. Phys. Chem. C* **2016**, *120*, 1523−1533.
(41) Song, J.; Zhao, H.; Sun, R.; Li, X.; Sun, D. An efficient hydrogen evolution catalyst composed of palladium phosphorous sulphide (PdP∼0.33S∼1.67) and twin nanocrystal Zn0.5Cd0.5S solid solution with both homo- and hetero-junctions. *Energy Environ. Sci.* **2017**, *10*, 225−235.
(42) Wang, J.; Li, B.; Chen, J.; Li, N.; Zheng, J.; Zhao, J.; Zhu, Z. Enhanced photocatalytic H2-production activity of CdxZn1−xS nanocrystals by surface loading MS (M = Ni, Co, Cu) species. *Appl. Surf. Sci.* **2012**, *259*, 118−123.
(43) Xu, X.; Lu, R.; Zhao, X.; Zhu, Y.; Xu, S.; Zhang, F. Novel mesoporous ZnxCd1−xS nanoparticles as highly efficient photocatalysts. *Appl. Catal., B* **2012**, *125*, 11−20.
(44) Wang, D. H.; Wang, L.; Xu, A. W. Room-temperature synthesis of Zn0.80Cd0.20S solid solution with a high visible-light photocatalytic activity for hydrogen evolution. *Nanoscale* **2012**, *4*, 2046−2053.
(45) Jakob, M.; Levanon, H.; Kamat, P. V. Charge Distribution between UV-Irradiated TiO2 and Gold Nanoparticles: Determination of Shift in the Fermi Level. *Nano Lett* **2003**, *3*, 353−358.
(46) Subramanian, V.; Wolf, E. E.; Kamat, P. V. Green Emission to Probe Photoinduced Charging Events in ZnO-Au Nanoparticles. Charge Distribution and Fermi-Level Equilibration. *J. Phys. Chem. B* **2004**, *107*, 7479−7485.
(47) Belcastro, M.; Marino, T.; Russo, N.; Toscano, M. The role of glutathione in cadmium ion detoxification: Coordination modes and binding properties − A density functional study. *J. Inorg. Biochem.* **2009**, *103*, 50−57.
(48) Li, X.; Yu, J.; Low, J.; Fang, Y.; Xiao, J.; Chen, X. Engineering heterogeneous semiconductors for solar water splitting. *J. Mater. Chem. A* **2015**, *3*, 2485−2534.
(49) Luo, X.; Wu, Z.; Liu, Y.; Ding, S.; Zheng, Y.; Jiang, Q.; Zhou, T.; Hu, J. C. Engineering Amorphous Carbon onto Ultrathin g-C3N4 to Suppress Intersystem Crossing for Efficient Photocatalytic H2 Evolution. *Adv. Mater. Interfaces* **2018**, *5*, No. 1800859.

https://doi.org/10.1021/acsomega.0c06038
ACS Omega 2021, 6, 13544−13553

(50) Jiang, W.; Liu, Y.; Wang, J.; Zhang, M.; Luo, W.; Zhu, Y. Separation-Free Polyaniline/TiO2 3D Hydrogel with High Photocatalytic Activity. *Adv. Mater. Interfaces* **2016**, *3*, No. 1500502.
(51) Yan, Z.; Yu, X.; Han, A.; Xu, P.; Du, P. Noble-Metal-Free Ni(OH)2-Modified CdS/Reduced Graphene Oxide Nanocomposite with Enhanced Photocatalytic Activity for Hydrogen Production under Visible Light Irradiation. *J. Phys. Chem. C* **2014**, *118*, 22896−22903.
(52) Zhang, W.; Hong, J.; Zheng, J.; Huang, Z.; Zhou, J. S.; Xu, R. Nickel-thiolate complex catalyst assembled in one step in water for solar H2 production. *J. Am. Chem. Soc.* **2011**, *133*, 20680−20683.
(53) Yang, H.; Jin, Z.; Fan, K.; Liu, D.; Lu, G. The roles of Ni nanoparticles over CdS nanorods for improved photocatalytic stability and activity. *Superlattices Microstruct.* **2017**, *111*, 687−695.
(54) Zhang, C.; Liu, H.; Wang, W.; Qian, H.; Wang, Y.; Zha, Z.; Zhong, Y.; Hu, Y.; Cheng, S. Scalable fabrication of ZnxCd1-xS double-shell hollow nanospheres for highly efficient hydrogen production. *Appl. Catal., B* **2018**, *239*, 309−316.
(55) Pei, L.; Liu, J.; Xu, Y.; Han, Y.; Wu, J.; Wang, Z.; Zhang, X. Hierarchical Zn1-xCdxS microclusters with superior visible-light-driven photocatalytic hydrogen generation performance. *J. Alloys Compd.* **2019**, *809*, No. 151869.
(56) Xu, H.; Yang, S.; Ma, X.; Huang, J.; Jiang, H. Unveiling Charge-Separation Dynamics in CdS/Metal−Organic Framework Composites for Enhanced Photocatalysis. *ACS Catal.* **2018**, *8*, 11615−11621.
(57) Tang, Y.; Li, X.; Zhang, D.; Pu, X.; Ge, B.; Huang, Y. Noble metal-free ternary MoS2/Zn0.5Cd0.5S/g-C3N4 heterojunction composite for highly efficient photocatalytic H2 production. *Mater. Res. Bull.* **2019**, *110*, 214−222.
(58) Shao, Z.; He, Y.; Zeng, T.; Yang, Y.; Pu, X.; Ge, B.; Dou, J. Highly efficient photocatalytic H2 evolution using the Ni2P-Zn0.5Cd0.5S photocatalyst under visible light irradiation. *J. Alloys Compd.* **2018**, *769*, 889−897.
(59) Tian, F.; Hou, D.; Tang, F.; Deng, M.; Qiao, X.; Zhang, Q.; Wu, T.; Li, D. Novel Zn0.8Cd0.2S@g-C3N4 core−shell heterojunctions with a twin structure for enhanced visible-light-driven photocatalytic hydrogen generation. *J. Mater. Chem. A* **2018**, *6*, 17086−17094.
(60) Zhao, S.; Xu, J.; Mao, M.; Li, L.; Li, X. NiCo2S4@Zn0.5Cd0.5S with direct Z-scheme heterojunction constructed by band structure adjustment of ZnxCd1-xS for efficient photocatalytic H2 evolution. *Appl. Surf. Sci.* **2020**, *528*, No. 147016.

https://doi.org/10.1021/acsomega.0c06038
ACS Omega 2021, 6, 13544−13553